Formulation of Curcumin in Folate Functionalized Polymeric Coated Fe_3O_4@Au Core-Shell Nanosystem for Targeting Breast Cancer Therapy

Adawiya J.Haider (adawiya.j.haider@uotechnology.edu.iq)
University of Technology https://orcid.org/0000-0002-2191-0500
Sharafaldin Al-Musawi
Mohammed J. Haider
Zeyad Yousif Abdoon Al-Shibaany

Research Article

Keywords: Fe3O4@Au, Au shell, nanoparticles, Drug delivery, Fe3O4 core, Chitosan, Breast cancer, Curcumin

Posted Date: February 7th, 2022

DOI: https://doi.org/10.21203/rs.3.rs-1324995/v1

Abstract

This research aims to design and synthesize a drug contained nanocomposite papered with a new combination of chitosan (CS)-coated magnetic-gold core-shell (Fe_3O_4@Au) as curcumin (CU) delivery to treat breast cancer (MDA-MB-231) and normal (MCF10A) cell lines. The CU drug was encapsulated in this nanosystem. Folate (Fol) functionalization of this nanosystem for targeting therapy purposes led to the construction of the final Fe_3O_4@Au-CS-CU-Fol nanoformulation. The SPION@Au was achieved using Pulsed Laser Ablation in Liquid (PLAL) procedure by the 530 nm wavelength with various laser fluence (1.8, 2.3, and 2.6) J/cm2. The polymeric coating, drug encapsulation, and Fol functionalization processes were performed due to reverse microemulsion methods. This nanosystem was characterized by a dynamic light scattering (DLS) Atomic Force Microscope (AFM), Field Emission Scanning Electron Microscopy (FESEM), High-Resolution Transmission Electron Microscopy (HRTEM), UV-Visible spectrophotometer, and vibrating sample magnetometry (VSM). A new type of CU-loaded nanocarrier was synthesized, and its anti-tumor properties were evaluated against breast cancer cell lines in both in vitro and in vivo conditions. The obtained mean size of Fe_3O_4@Au nanoparticles (NPs) was 52.37, 60.24, and 72.45 nm at 1.8, 2.3, and 2.6 J/cm2, respectively. The MTT (3-(4,5-dimethylthiazol-2-yl)-2,5-diphenyltetrazolium bromide) assay of drug-loaded NPs on the MDA-MB-231 cell line proved that the CU cytotoxicity effect could enhance when encapsulated in Fe_3O_4@Au-CS-Fol nanocarrier compared with void CU. On the other hand, the flow cytometry charts presented that this nanoformulation can enhance the remedial properties of CU due to apoptosis stimulation in the MDA-MB-231 cell line. The real-time polymerase chain reaction (PCR) analysis confirmed the activation of apoptosis in the cells treated with the Fe_3O_4@Au-CS-CU-Fol. The in vivo evaluation of the Fe_3O_4@Au-CS-CU-Fol nanosystem proved that the tumor volume reduces in a certain time. Close inspection of results confirmed that Fe_3O_4@Au-CS-CU-Fol exerts a significant chemo-preventive effect on breast cancer through cell viability index, apoptosis stimulation, and anti-tumor activity.

1. Introduction

Surgery, chemotherapy, and radiation therapy were expanded for the treatment of various cancers. Still, the natural cells are also affected due to subjection to these anti-cancer treatments and lead to cell-damaging or, subsequently, cell death [1, 2]. There have been numerous research efforts to enhance cancer therapeutic efficiency to decrease destructive properties on natural cells. Construction of Fe_3O_4@Au nanocomposite has appeared as a striking tactic over the last years for their broad applications in the medical and biological fields, comprising drug target therapy in cancer treatment, diagnosis, and bioseparation [3–6]. The nanomaterials are a strong applicable device to decrease the radiation side effects in the natural cells against the cancer cell [7–10]. The NPs present smart and unique material characteristics with noticeable variations compared to those mass states due to their nano-scale size [11]. The Au functionalizing of Fe_3O_4 led to its stability increment and developed their dispersion characteristic [12, 13]. Fe_3O_4@Au core-shell nanocomposites have remarkable importance due to their diagnostic properties [14]. The protection of Fe_3O_4 from oxidation processes is one of these

advantages. Au shell is an excellent covering material due to its specific surface potency and functionalization with a specific chemical agent. [15, 16]. The PLAL strategy is a supple and immaculate method for the construction of core-shell nanocomposites [17]. This technique is one of the top-down nanomaterials synthesis strategies carried out in liquid conditions and to laser radiation interaction with a solid material. In this method, the laser pulse is concentrated on metallic material in a specific liquid solution that generates NPs colloids [18–20]. PLAL strategy is a noteworthy perspective due to its simplicity and pure production output. The normal pressure with ambient temperature is sufficient conditions for performing this process. We can regulate the experimental parameters, such as the laser conditions, targeted material kinds, solutions types, and external environment. This adjustment gives the controlling capability for the different material characteristics, such as structures and size [21–25]. Nanotechnology improved the drug delivery technique to decrease the drug side effects using different types of nanocarriers. CU has anti-cancer properties, but its utilisation is restricted due to its remarkable water insolubility and poor bioavailability. We designed a novel drug delivery system to solve these problems with CS Au-coated SPION (Fe_3O_4@Au-CS-CU-Fol NPs) to confirm CU potential as a potent and powerful anti-cancer agent applied to breast cancer therapy. This research is to design and synthesise a novel drug nanocarrier combination (Fe_3O_4@Au-CS-CU-Fol NPs) using the PLAL process as a drug delivery system to treat breast cancer (MDA-MB-231) and normal (MCF10A) cell lines.

2. Materials And Methods

2.1 Synthesis of Fe_3O_4@Au nanostructure

SPION@Au was fabricated following a previous procedure [13]. The Fe and Au plates were purchased from sigma-aldrich (St. Louis, MO, USA). Figure 1 exhibits the schematic diagram of experimental details using the PLAL method for core-shell nanoparticles synthesis in colloidal solution. The Nd-YAG laser system is used in this experiment. This nanosecond laser system has a repetition rate of 1-6 Hz in optimal 10 ns pulse duration. The laser wavelengths are 1064 nm' fundamental harmonic generation', 532 nm' second harmonic generation SHG" using a KDP crystal (K. potassium, D. deuterium, P. phosphate (sigma-aldrich)). The metallic targeted plates (Fe and Au plates) is secured separately by a fixture inside the flask and immersed at 12 mm depth in the internal solution of the flask. The ablation process was typically done at room temperature. The laser beam spot size on a metal plate's surface is different in the width of 1.5 mm in diameter by alternating the interval between the metal plate and the focusing lens. First the ablation process is typically done on Fe-plate for 1 minute. The color of water turns to gray indicated the Fe ion liberation from Fe-plate in solution. The Fe ions were oxidized rapidly in water environment and turns to Fe_3O_4. The formed Fe_3O_4 changed the watercolour to grey, proving the Fe_3O_4 NPs existence. Fe_3O_4@Au core-shell NPs were synthesized due to PLAL. The three various laser fluences were 1.8 J/cm^2, 2.3 J/cm^2, and 2.6 J/cm^2.

2.2 Preparation of CU loaded Fe_3O_4@Au-CS-Fol NPs

10 mg of (CS) powder (Sigma-Aldrich (St. Louise, MO, USA)) dissolved in 100 ml of distilled deionized water (DDW) and glacial acetic acid (1:1 V/V). CS solution adds to Fe_3O_4@Au NPs solution, and then 15 mg CU (Sigma-Aldrich (St. Louise, MO, USA))was added to the Fe_3O_4@Au-CS. Then 5ml Fol (Merck, Germany) was mixed with Fe_3O_4@Au-CS-CU nanosystem. Continuously stirring at 800 rpm/min for 10 h caused it to form the nanostructure microemulsion. The microsyringe filter was used for its filtration to obtain the pure Fe_3O_4@Au-CS-CU-Fol nanosystem solution [13].

2.3 Characterization of Fe_3O_4@Au-CS-CU-Fol NPs

The nanosystem was evaluated using DLS (MALVERN, Nano S, London, UK), VSM (Lakeshore 7404, USA), UV-Visible spectrophotometer (Aquarius 7000, Italia), XRD (SIEMENS-D5000, Karlsruhe, Germany), FESEM (Hitachi S-4160, Japan) and HRTEM (Carl Zeiss AG - Zeiss EM900, Germany). The Fe_3O_4@Au-CS-Fol drug encapsulation efficiency was obtained using the mentioned equation [1]:

Encapsulation efficiency (%) = [(drug fed – drug loss) / (drug fed)] × 100% Eq. (1)

2.4 Drug Release Assay

Two phosphates (pH=7.4) and citrate (pH=5.4) buffered in 0.01 M concentration were utilized at 37 ˚C to calculate CU liberation behaviour from its nanocarrier. Nanosystem solution (1ml) was poured into the dialyze bag (Sigma-Aldrich (St. Louise, MO, USA)). The nanosystem-included bags were placed separately in the 100ml phosphate and citrate buffers. The Tween 80 (Sigma-Aldrich (St. Louise, MO, USA)) emulsifier was utilized to inhibit drug-released sedimentation. The sampling processes were performed at various times (0, 4, 8, 12, 24, 48, 72, and 96 h). The 500µl of each buffer was aliquoted and dissolved in 2 ml Dimethyl sulfoxide (DMSO) (Merck, Germany) and, consequently, freeze-dried. Finally, fluorescence spectroscopy was utilized for the calculation of drug liberation amounts. The result was calculated by the mentioned:

$$R = \frac{V\sum_{i}^{n-1} C_i + V_o C_n}{m_{drug}} \quad \text{Eq. (2)}$$

In this equation, R is the CU release ration, the concentration of CU indicated by Ci and Cn, the sampling amount and initial volume of CU presented using V and V0, respectively. The CU mass in NPs exhibited by mdrug and the sampling times indicated by *i* and *n*. Finally, the sediment material was washed and resuspended in DDW.

2.5. Cell Culture

MDA-MB-231and MCF-10A cell lines (purchased from the American Type Culture Collection (ATCC, Manassas, VA, USA) were cultured in 100 mL culture flasks using Dulbecco's modified Eagle medium (DMEM) cell culture medium, 10% phosphate-buffered saline (PBS), and 1% penicillin-streptomycin (1 × 10^4 units per mL). The culture was incubated at 37 ◦C in a humidified atmosphere containing 5% CO2.

2.6 Cell Internalisaion Assay

Regarding cell internalization rate studies, 20 µM of drug-loaded nanocarrier was used to treat the cultured cells for 4 h. The cell surfaces were washed with phosphate buffer saline (PBS) after discarding the whole drug-contained medium. The fluorescence imaging process was carried out via a fluorescence microscope (Hitachi, Japan). The same cells in other plates were subjected to an equal dose of free CU solution for fluorescence microscopy study to evaluate the Fe_3O_4@Au-CS-CU-Fol nanocarrier efficiency in enhancing the capability of the CU bioavailability and solubility.

2.7 MTT Assay

In preparing the 5 mg/ml MTT (Sigma-Aldrich (St. Louise, MO, USA)) solution for the MTT test, 96 well plates were filled with 10^4 cells per well. Each well was fed by 200 µl of Dulbecco's Modified Eagle's medium (DMEM) (Merck, Germany), and the cells were allowed to divide and grow for 24 h. The 10–60 µM concentrations of the void drug, drug-loaded nanocarrier and the NPs alone dissolved into DMSO (Merck, Germany) and added into wells. The MTT test was accomplished at 24 and 48 h periods after treatment and in triplicate wells and frequented three times. MTT solution was added to 24 and 48 h treated cells in 2 h incubation. Subsequently, the entire solutions were removed and then substituted with 100 µl DMSO for each well. The 96 wells plates were put in the shaker for 15 minutes then estimated by enzyme-linked immunosorbent assay (ELISA) reader (BioTek Power Wave XS).

2.8 Flow Cytometry

The 6 well plates were utilized for apoptosis induction assay and poured 10^4 cells in each well. The cells were treated separately with the void drug, drug-loaded nanocarrier, and the NPs alone at 48h. Apoptosis induction was calculated by the Annexin V-FITC Apoptosis Detection Kit (Beyotime, Biotechnology Co., Ltd. Nantong, China). After 48 h, the cells were collected from wells and centrifuged at 300 g for 4 minutes. The supernatant was removed, and the cells were suspended in 600 µl of 1X binding buffer. PI and Annexin V–FITC (5 µl of each) were applied separately for treating the obtained solutions. Then the solution was mixed and incubated for 12 min at ambient temperature and poured into Fluorescence-activated cell sorting (FACS) tubes. Consequently, the FACS tubes were analyzed through the FACScan Flow Cytometer (Becton Dickinson, Oxford, UK).

2.9 RT-PCR

2.9.1 Total RNA Isolation for complementary DNA synthesis

All RNA was separated from MDA-MB-231 cells after 48 h treatment, utilizing TRIzol reagent following the manufacturer's instructions (Invitrogen Life Technologies, UK). RNA quantity was measured by calculating OD 260/280. The A260/A280 proportion of isolated RNA was about 1.7 to 1.8, measured utilizing a Nanodrop-2000c spectrophotometer (Thermo Scientific, USA). Entire RNA was processed directly to cDNA by reverse transcription with a cDNA Synthesis Kit (Fermentas, Germany) in a 30 µl total volume reaction. Temporarily, a reaction mixture of 3.5 µg total RNA, 0.5 µl random hexamer, 0.5 µl Oligo (dT) primers and 13.5 µl DEPC of treated water on dry ice was mixed and incubated at 60 ºC for 5 min and stored 1 min on dry ice. Then 6 µl (5X) buffer, 1.5 µl (20 u/µl) RNase inhibitor and 3 µl (10 mM) dNTP

Mix was added and incubated at 25 ºC for 6 min. Afterward, 1.5 µl M-MuLV (20 u/µl) was added and incubated at 25 ºC for 6 min and again incubated at 42 ºC for 1h. The reaction was ended by heating at 75 ºC for 5 min. cDNA was instantly applied in the RT-PCR reaction.

2.9.2 Quantitative RT-PCR reaction

Primer designing for BAX and BCL2 genes was carried out using software primer express. The β-actin Forward:5'-CTGGCACCCAGCACAATG-3', Reverse: 5'-GCCGATCCACACGGAGTACT-3', BAX Forward: 5'-AGCTGCAGAGGATGATTGC-3', Reverse: 5'-GTTGAAGTTGCCGTCAGAAA-3' and Bcl-2 Forward: 5'-TGCCTTTGTGGAACTGTACG-3', Reverse: 5'-GGCCAAACTGAGCAGAGTC-3' mentioned in Table 1. The expression levels of BAX and Bcl-2 were studied with Real-Time PCR on an ABI prism 7500 sequence detection system (Applied Biosystems, USA). Beta-actin was considered as a reference control gene. 10 µl of the SYBR Green-I dye (Applied Biosystems, USA), 0.5 µl of each of the specific primers (with a concentration of 50 nM), and 5 µl of cDNA were added to PCR microtube for the amplification reaction. RT-PCR reaction was carried out as mentioned in Table 2.

2.10. In Vivo Study

2.10.1. Animal Use

NOD.CB17-Prkdcscid/J mice 6–8 weeks old and weighing 25 g were acquired from the animal house. The guideline approved animal care and use of Animal Care and Research Committee of Al-Qasim Green University (ethics committee approval code: 533FD2) was adopted from the guideline for the care and use of laboratory animals. All in vivo protocols and methods were performed by pertinent guidelines and regulations. Moreover, all experimental procedures were confirmed by an Animal Care and Research Committee of Al-Qasim Green University.

2.10.2. Tumor Volume and Survival Rate Studies

The mice were anaesthetized with 80%; tiletamine/zolazepam 32 mg/kg and xylazine 8 mg/kg, during intraperitoneal injection. A total of 1 × 106 MDA-MB-231 exponentially growing cells/200 µL of PBS-free medium were injected subcutaneously (s.c.) in NOD.CB17-Prkdcscid/J mice. Tumor mass was con□rmed on day 8 due to the fast growth and offensive characteristics of the MDA-MB-231 cell line. The animals were divided randomly into four groups (n = 7 per group), including two test groups intravenously receiving 12.5 mg/kg body weight CU loaded NPs and free CU for 3 weeks and two control groups including Fe_3O_4@Au-CS-Fol and PBS.

Tumor volume (mm3) was calculated three times per week using a digital Vernier caliper (Mitutoyo, Japan) using the Equation (2).

$$Tumor\ volume = \frac{1}{2}\left[Tumor\ length \times (Tumor\ width)^2\right] \quad (2)$$

Table 1
Primers used for β-Actin, BAX, and BCL-2 genes in the present study.

Primer Name	Primer Sequence Oligo sequence F (5' ◊ 3')	Primer Sequence Oligo sequence R (5' ◊ 3')
β-actin	CTGGCACCCAGCACAATG	GCCGATCCACACGGAGTACT
BAX	AGCTGCAGAGGATGATTGC	GTTGAAGTTGCCGTCAGAAA
BCL-2	TGCCTTTGTGGAACTGTACG	GGCCAAACTGAGCAGAGTC

Table 2
Temperature, time, and the number of cycles for each step.

Step	Temperature	Time	Cycles
Initial Denaturation	95°C	10 min	1
Denaturation	95°C	15 sec	48
Annealing	60°C	1 min	
Melting curve analysis	95°C	5 sec / step	1

2.11 Statistical Analysis

SPSS software (Version 24) and was used for statistical analyses and graphical representations, respectively. p values less than 0.05, 0.001, and 0.001 were assumed statistically significant. The data are shown here as mean ± SD of 3 separately tested.

3. Results

3.1 Optical properties results

From the spectrum of ultraviolet rays, it is possible to estimate how much the grain size of the materials prepared are iron and gold by displacing the absorption peak. If towards long wavelengths tend to create large granular volumes and if towards short wavelengths tend to create small granular volumes, it is because the plasmon band shifts toward a higher wavelength (a redshift) with enhancing practical diameter size according to reference [13]. Fig. 2 shows the absorption spectrum of Fe_3O_4@Au NPs prepared by the 1.8, 2.3, and 2.6 J/cm^2 laser fluence shootings. The results apear the three peaks absorption bands with Fe_3O_4 NPs core at 226, 228, and 232 nm with laser fluences 1.8, 2.3, and 2.6 J/cm^2 respectively. While the surface plasmon resonance (SPR) of the gold shell presented at absorption band at 505, 509, and 535 nm with laser fluences 1.8, 2.3, and 2.6 J/cm^2 respectively. These results are coincident with [13]. Curves showed a redshift toward longer wavelengths by increasing particle size with laser fluence raises [26]. The size, distribution, and charge of NPs (that synthesized under 1.8 J/cm^2 laser

fluence) were estimated using DLS (Malvern Zetasizer ZS, Malvern, UK). The findings presented the NPs distribution, charge and size were 0.080, -46 Mv, and ~ 190 ± 17 nm, respectively (Figure 3a, b). The diameter size of NPs is the most remarkable factor for adjusting the NPs compatibility and activity characteristics. The NPs diameter size is also a notable parameter for nanocarrier stability [17]. Earlier, N. Kumar et al. [14] presented vincristine-loaded folate-decorated chitosan NPs with a spherical-like structure due to vincristine loading. The magnetic properties of Fe_3O_4@Au-CS-CU-Fol were determined using VSM. As exhibited in Fig. 4 uncoated Fe, Fe_3O_4@Au, Fe_3O_4@Au-CS, Fe_3O_4@Au-CS-CU, and Fe_3O_4@Au-CS-CU-Fol were studied magnetically. The saturation magnetization of the uncoated Fe was 62 emu/g, while in the case of Fe_3O_4@Au, it was 58 emu/g and 45, 38 and 30 in Fe_3O_4@Au-CS, Fe_3O_4@Au-CS-CU, and Fe_3O_4@Au-CS-CU-Fol, respectively. This reduction in saturation magnetisation was due to covering the remarkable amount of gold, chitosan, and folic acid in the Fe nanoformulation [29]. The UV visible curve of 1.8 j/cm2 didn't reach zero because of the high-level aggregation/polydispersity of the nanoparticle compare with the other two nanoparticles (synthesized using 2.3, and 2.6 J/cm2 fluences) that their curves reached zero. These findings were in agreement with the DLS results as shown in supplementary Fig. 1a,b and c. The supplementary Fig. 1a shows the Polydispersion rate of 0.211 which is more than two other nanoparticles (in 2.3, and 2.6 J/cm2 fluences) were in agreement with the DLS results as shown in Fig. 3a and b. The obtained mean size of Fe_3O_4@Au nanoparticles (NPs) was 52.37, 60.24, and 72.45 nm at 1.8, 2.3, and 2.6 J/cm2, respectively (Table 3).

3.2 Chemical composition and electron microscopy of core-shell Fe_3O_4@Au NPs

The powder X-ray diffraction (XRD) patterns of the SPION and SPION@Au core-shell NPs are shown in Figure 5. The raw SPION (311) peak has a diffraction angle of 39.51, indicating that the SPION composition is magnetite before the Au shell is reduced. The XRD signals shift to (111) Au shell formation on the surface of SPION after it is encapsulated with Au. Because of the heavy atom effect, the gold layer shielded the XRD signals of the Fe3O4 core.

Table 3
Fe_3O_4@Au diameter size obtained different fluence of 1.8, 2.3 and 2.6 J/cm^2 respectively.

Laser Sample	fluence (J/cm^2)	Nanoparticle's diameter size (nm)
S1	1.8	52.37
S2	2.3	60.24
S3	2.6	72.45

Figure 6 indicates a suitable uniform dispersion of spherical NPs. The SEM micrograph of Fe_3O_4@Au core-shell nanostructure is presented in Figure 6a. The figures present an average size of 52.37 nm for the prepared NPs. In comparison, Figure 6b revealed the diameter sizes of 187.8 nm for the prepared Fe_3O_4@Au-CS-CU-Fol NPs [31-32].

Figure 7 illustrates TEM images of NPs prepared with a laser fluence of 1.8 J/cm2. Figure 7a shows Fe_3O_4@Au NPs, which have a uniform average size of around 52.37 nm and a globular shape as core-shell. The Au NPs shell has an average size of 28.15 nm as the shell is brighter than the Fe NPs core (darker part) agrees with reference [33]. Figure 7b shows that the Fe_3O_4@Au-CS-CU-Fol NPs with enlarged structure have an average size of around 189.2 nm and a spherical shape.

3.3 Encapsulation Efficiency

The obtained nanoformulation solution was centrifuged at 14000 rpm for 15 minutes. The nanoformulation was precipitated after centrifugation processes, and then the supernatant will contain free unloaded CU drug. The supernatant was collected, freeze-dried, and dissolved in DMSO and subsequently estimated using a spectrophotometer at 420 nm. The obtained results presented the free unloaded CU drug. Calculating the loaded CU drug in nanoformulation was readily possible by subtracting the free drug from the total initial given value. The Fe_3O_4@Au-CS-CU-Fol nanocarrier showed 72% encapsulation efficiency for curcumin. The nanoformulation presented noticeable drug durability and proper colloidal stability.

3.4 Release Profile

Drug releases from its nanoformulation over a 96 h period indicate that the release period in pH 5.4 is faster than pH 7.4, as shown in Figure 8. These data presented the controlled liberation behavior of this nanoformulation due to the degradability characteristics of chitosan in acidic pH. These data were in confidence with the same CU nanoformulated chitosan-coated magnetic NPs [1,5,15].

3.5 Cell uptake Study

Evaluation of CU uptake into cancer MDA-MB-231 cell line, and its innate fluorescence characteristic, were carried out using fluorescence microscopy. Figure 9 showed the CU treatment of cells in its free and nanoformulated form that indicated a green color after its enhanced solubility caused cell uptake. On the other hand, in the void CU treated MDA-MB-231 cells, the green aggregated particles were shown in intercellular space because of their insolubility in aqueous conditions [1].

3.6 MTT Assay

The cell viability percentage of curcumin (CU) was estimated using the MTT test on MDA-MB-231 and MCF10A cell lines. This experiment was accomplished in a 24 and 48 h period and was indicated in Figure 10. Both cell lines were treated with several concentrations (10–60 μM) of Fe_3O_4@Au-CS-CU-Fol for 24 and 48 h. However, about the free CU and unloaded NPs, the data were estimated in 48 h period only. Fe_3O_4@Au-CS-CU-Fol nanoformulation noticeably $P<0.01$ prevented the cancer MDA-MB-231 cells viability compared with bare NPs and free CU but did not exhibit any significant difference in cell viability after treating cancer MDA-MB-231 and normal MCF10A cell lines. Both free CU and bare NPs treatment did not present any significant cytotoxic properties in all employed doses. The cytotoxicity evaluation study revealed that the IC50 ratio of Fe_3O_4@Au-CS-CU-Fol for MDA-MB-231 cell lines within 24 h and 48 h

was 54 μM and 28 μM, respectively. These results were in adaptation with the data of the investigation of the same treatment results of CU loaded in chitosan-coated magnetic NPs [33-35].

3.7 Flow Cytometry.

A noticeable increase was exhibited in the rate of apoptotic cancer cells compared to normal cells (Figure 11). As shown in Figure 11a, the normal cells were not affected significantly by Fe_3O_4@Au-CS-CU-Fol, while it exhibited remarkable apoptosis in cancer cells. In Figure 11b, the Fe_3O_4@Au-CS-Fol did not show any apoptotic induction in the various treatment doses on the MDA-MB-231 cancer cell line, which confirmed that the bare unloaded Fe_3O_4@Au-CS-Fol does not stimulate any apoptosis on both MDA-MB-231 and MCF10A cell lines. The data have also presented that void CU did not exhibit any apoptotic induction in the MDA-MB-231 cancer cell line. Additionally, Fe_3O_4@Au-CS-CU-Fol nanoformulation resulted in 18.39% apoptosis induction, by 6.38% early apoptosis (Q3 square) and 13.1% late apoptosis (Q2 square), respectively. On the other hand, the cytotoxic rate of free CU and unloaded NPs on the MDA-MB-231 cells was insignificant. These data were adjacent to the results of the similar CU-loaded chitosan-coated magnetic-gold core-shell that was synthesized by the microemulsion method [15, 34].

3.8 Gene expression study using RT PCR

RT PCR analyzed the BAX and BCL-2 gene expression to estimate the void CUR and FOL-CUR-PU nanoformulation effect on the MDA-MB-231 cell line. The melting curve analysis was performed, verifying the correct product according to its specific melting temperature (Tm). CU induces this release by inducing BAX (pro-apoptotic) and Bcl-2 (anti-apoptotic) inhibition. Therefore, we evaluate the expression level of mentioned genes in the MDA-MB-231 cell line after treatment with Fe_3O_4@Au-CS-CU-Fol nanoformulation in comparison to the Fe_3O_4@Au-CS-Fol NPs and void CU. Statistical analysis of RT-PCR results illustrates that after treatment, the Fe_3O_4@Au-CS-CU-Fol noticeably reduced the expression of Bcl-2 by 0.34 fold ($P<0.001$) of the control group (untreated). Moreover, Fe_3O_4@Au-CS-CU-Fol noticeably up-regulated ($P<0.0001$) the expression of BAX by 2.45 fold of normal levels, in comparison to void CU (Fig. 12).

3.9 In vivo

The Fe_3O_4@Au-CS-CU-Fol nanosystem effect was studied in vivo using nude mice (Figure 13). The guideline approved animal care and use of Animal Care and Research Committee of Al-Qasim Green University (ethics committee approval code: 533FD2) was adopted from the guideline for the care and use of laboratory animals. All in vivo protocols and methods were performed by pertinent guidelines and regulations. Moreover, all experimental procedures were con□rmed by an Animal Care and Research Committee of Al-Qasim Green University.

The Fe_3O_4@Au-CS-CU-Fol nanosystem, Fe_3O_4@Au-CS-Fol nanocarrier, free CU, and PBS as controls were injected intravenously to female nude mice. The mice body weight calculation confirmed the insignificant difference of mice compared to control—PBS injected mice. Additionally, no death was observed in mice

during the study period. The finding proved the anti-tumor potency of Fe_3O_4@Au-CS-CU-Fol against control, Fe_3O_4@Au-CS-Fol nanocarrier, and free CU. In Figure 13, as presented in the curve, the Fe_3O_4@Au-CS-CU-Fol significantly decreases the mean tumor volume in nude mice. In contrast, the other treatments (control, Fe_3O_4@Au-CS-Fol nanocarrier, and free CU) indicated enhancement of tumor volume.

4. Conclusion

This research improved a smart nanostructure of CU-loaded metal-polymeric as a possible tumor chemo-therapeutic agent to enhance CU anti-tumor properties. In this work, the Fe_3O_4@Au nanosystem was prepared by the PLAL procedure with various laser fluence 1.8, 2.3, and 2.6 J/cm2. CU was loaded into Fe_3O_4@Au-CS, and then Fol functionalized to create the Fe_3O_4@Au-CS-CU-Fol nanosystem. The characterization was carried out by different methods, TEM, SEM, and AFM, to confirm the accurate preparation of the Fe_3O_4@Au-CS-CU-Fol nanosystem. Furthermore, the cell internalization, release profile, MTT test, and apoptosis induction by flow cytometry were utilized to survey the anti-tumor properties of the Fe_3O_4@Au-CS-CU-Fol nanosystem. The findings proved that the Fe_3O_4@Au-CS-CU-Fol has a noticeable enhancement effect in cell death and apoptosis induction compared to unloaded Fe_3O_4@Au-CS-Fol nanocarrier or free drug on the MDA-MB-231 cell line. The prepared Fe_3O_4@Au-CS-CU-Fol nanoformulation exhibited a nano-scale size, controlled liberation, and notable stability. The findings demonstrated that Fe_3O_4@Au-CS-CU-Fol NPs nanoformulation stimulates an increase in MDA-MB-231 cell death and leads to an 18.5% apoptosis rate. The in vivo result of the Fe_3O_4@Au-CS-CU-Fol nanosystem proved that the tumor volume reduced over time and even reached a minimal size.

Declarations

Author Contributions: Conceptualization and methodology, A.J.H and S.A.-M; formal analysis, A.J.H and S.A.-M; investigation and data curation, A.J.H and S.A.-M; validation, A.J.H and S.A.-M; formal analysis, A.J.H and S.A.-M; visualization, A.J.H and S.A.-M; writing—original draft preparation, A.J.H and S.A.-M; writing—review and editing, Z.Y.A, A.J.H and S.A.-M.; supervision, A.J.H and S.A.-M; project administration A.J.H, S.A.-M and M.J.H;. All authors have read and agreed to the published version of the manuscript.

Funding: This research received no external funding.

Conflicts of Interest: The authors declare no conflict of interest.

References

1. S. Al-Musawi, M.J. Kadhim, N.K.K. Hindi, Folated-nanocarrier for paclitaxel drug delivery in leukemia cancer therapy. J. Pharm. Sci. & Res. **10**(4), 749–754 (2018)
2. A. Urruticoechea et al., "Recent advances in cancer therapy: an overview". Curr. Pharm. Des. J. **16**(1), 3–10 (2010)

3. M.A. Al-Kinani, A.J. Haider, & Al-Musawi. "Study the Effect of Laser Wavelength on Polymeric Metallic Nanocarrier Synthesis for Curcumin Delivery in Prostate Cancer Therapy: In Vitro Study". J. Appl. Sci. Nanatechnol. **1**(1), 43–50 (2021). doi:10.53293/jasn.2021.11023
4. S. Al-Musawi, S. Albukhaty, H. Al-Karagoly, G.M. Sulaiman, M.S. M S Jabir, H. Naderi-Manesh, dextran-coated superparamagnetic nanoparticles modified with folate for targeted drug delivery of camptothecin. Adv. Nat. Sci: Nanosci. Nanotechnol **11**(4), 045009 (2020). doi:10.1088/2043-6254/abc75b
5. M.A. Al-Kinani, A.J. Haider, S. Al-Musawi, Design, Construction and Characterization of Intelligence Polymer Coated Core-Shell Nanocarrier for Curcumin Drug Encapsulation and Delivery in Lung Cancer Therapy Purposes. J. Inorg. Organomet. Polym. **31**, 70–79 (2021). doi:10.1007/s10904-020-01672-w
6. A.J. Haider, M.J. Haider, M.S. Mehde, A review on preparation of silver nano-particles, J. Amer. Inst.of Phys., (2018)
7. L. Salim Albukhaty, H. Al-Bayati, Al-Karagoly, S. Al-Musawi (2020): Preparation and characterization of titanium dioxide nanoparticles and in vitro investigation of their cytotoxicity and antibacterial activity against Staphylococcus aureus and Escherichia coli, Animal Biotechnology, DOI: 10.1080/10495398.2020.1842751
8. S. Al-Musawi, S. Albukhaty, H. Al-Karagoly, G.M. Sulaiman, M.S. Alwahibi, Y.H. Dewir, D.A. Soliman, H. Rizwana, Antibacterial Activity of Honey/Chitosan Nanofibers Loaded with Capsaicin and Gold Nanoparticles for Wound Dressing. Molecules **25**, 4770 (2020). doi:10.3390/molecules25204770
9. I.Y. Goon, L.M.H. Lai, M. Lim, P. Munroe, J.J. Gooding, R. Amal, Fabrication and dispersion of gold-shell-protected magnetite nanoparticles: systematic control using polyethyleneimine. Chem. Mater. J. **21**(4), 673–681 (2009)
10. W. Lingyan et al., "Monodispersed core-shell Fe_3O_4@Au nanoparticles". Phys. Chem. B J. **109**, 21593–21601 (2005)
11. S. Albukhaty, S. Al-Musawi, S. Abdul Mahdi, G.M. Sulaiman, M.S. Alwahibi, Y.H. Dewir, D.A. Soliman, H. Rizwana, Investigation of Dextran-Coated Superparamagnetic Nanoparticles for Targeted Vinblastine Controlled Release, Delivery, Apoptosis Induction, and Gene Expression in Pancreatic Cancer Cells. Molecules **25**, 4721 (2020). doi:10.3390/molecules25204721
12. S. Al-Musawi, S. Ibraheem, S.A. Mahdi, S. Albukhaty, A.J. Haider, A.A. Kadhim, K.A. Kadhim, H.A. Kadhim, H. Al-Karagoly Smart Nanoformulation Based on Polymeric Magnetic Nanoparticles and Vincristine Drug: A Novel Therapy for Apoptotic Gene Expression in Tumor. Life 2021, 11, 71. https://doi.org/10.3390/life 11010071
13. M.A. Al-Kinani, A.J. Haider, S. Al-Musawi Design and Synthesis of Nanoencapsulation with a New Formulation of Fe@Au-CS-CU-FA NPs by Pulsed Laser Ablation in Liquid (PLAL) Method in Breast Cancer Therapy: In Vitro and In Vivo. Plasmonics (2021). https://doi.org/10.1007/s11468-021-01371-3

14. N. Kumar, R.K. Salar, M. Prasad, K. Ranjanc, Synthesis, characterization and anti-cancer activity of vincristine loaded folic acid-chitosan conjugated nanoparticles on NCI-H460 non-small cell lung cancer cell line. Egypt. J. Basic. Appl. Sci. **5**, 87–99 (2018)
15. S. Al-Musawi, A.J. Hadi, S.J. Hadi, N.K.K. Hindi, Preparation and Characterization of Folated Chitosan-Magnetic Nanocarrier for 5-Fluorouracil Drug Delivery and Studying its Effect in Bladder Cancer Therapy. J. Global Pharma Tech. **11**(7), 628–637 (2019)
16. M. Mofazzal Jahromi, S. Al-Musawi, M. Pirestani, M. Fasihi Ramandi, K. Ahmadi, H. Rajayi, M. Hassan, Z. Kamali, M. Mirnejad, R. 'Curcumin-loaded Chitosan Tripolyphosphate Nanoparticles as a safe, natural and effective antibiotic inhibits the infection of Staphylococcus aureus and Pseudomonas aeruginosa in vivo'. Iran. J Biotech **12**(3), e1012 (2014). doi:10.15171/ijb.1012
17. A.J. Haider, A.J. Mohammed, S.S. Shaker, K.Z. Yahya, M.J. Haider, Sensing characteristics of nanostructured SnO2 thin films as glucose sensor. Energy Procedia **119**, 473–481 (2017). doi:10.1016/j.egypro.2017.07.056
18. V. Amendola, G.A. Rizzi, S. Polizzi, M. Meneghetti, "Synthesis of gold nanoparticles by laser ablation in toluene: quenching and recovery of the surface plasmon absorption". Phys. Chem. B J. **109**(49), 23125–23128 (2005)
19. S. Georgiou, A. Koubenakis, "Laser-induced material ejection from model molecular solids and liquids: mechanisms, implications, and applications". Chem. Reviews J. **103**(2), 349–393 (2003)
20. L. Zhigilei, B. Garrison, "Mechanisms of laser ablation from molecular dynamics simulations: dependence of the initial temperature and pulse duration". Appl. Physices A **69**, S75–S80 (1999)
21. Z. Haibo, D. Xi-Wen, C. Subhash, A. Sergei, Y. Shikuan, H. Jianping, C. Weiping, " Nanomaterials via Laser Ablation/Irradiation in Liquid: A Review" Advanced Functional Materials Journal **22**, 1333–1353 (2012)
22. M.J. Al-Awady, A.A. Balakit, S. Al-Musawi, M.J. Alsultani, A.M. Ahmed Kamil. Investigation of Anti-MRSA and Anticancer Activity of Eco-Friendly Synthesized Silver Nanoparticles from Palm Dates Extract. Nano Biomed. Eng. 2019; 11(2):157–169. doi: 10.5101/nbe. v11i2.p157-169
23. M. Ma, H. Chen, Y. Chen, X. Wang, F. Chen, X. Cui, J. Shi, Au capped magnetic core/mesoporous silica shell nanoparticles for combined photothermo-/chemo-therapy and multimodal imaging. Biomaterials J. **33**, 989–998 (2012)
24. M. Hu, H. Petrova, J. Chen, J. McLellan, A. Siekkinen, M. Marquez, L. Xingde, X. Younan, V. Gregory, Hartland "Ultrafast laser studies of the photothermal properties of gold nanocages". Phys. Chem. B J. **110**, 1520–1524 (2006)
25. A.J. Haider, A.D. Thamir, D.S. Ahmed, M.R. Mohammad Deposition of silver nanoparticles on multiwalled carbon nanotubes by chemical reduction process and their antimicrobial effects. AIP Conference Proceedings 1758, 030003 (2016); doi: 10.1063/1.4959399
26. G. Guillermo, G. Andres, M. Luis, Reshaping, Fragmentation, and Assembly of Gold Nanoparticles Assisted by Pulse Lasers. Acc. Chem. Res. J. **49**(4), 678–686 (2016)

27. W.J. Al-Kaabi, S. Albukhaty, A.J.M. Al-Fartosy, H.K. Al-Karagoly, S.M. Al-Musawi, G.M. Sulaiman, Y.H. Dewir, M.S. Alwahibi, D.A. Soliman Development of Inula graveolens (L.) Plant Extract Electrospun/Polycaprolactone Nanofibers: A Novel Material for Biomedical Application. Appl. Sci. 2021, 11, 828. https://doi.org/ 10.3390/app11020828
28. E. Tatiana, "On Nanoparticle Formation by Laser Ablation in Liquids" Physical Chemistry C. Journal **115**(12), 5044–5048 (2010)
29. Karamipour S., Sadjadi M., & Farhadyar N., "Fabrication and Spectroscopic Studies of Folic Acid-Conjugated Fe_3O_4@Au Core–Shell For Targeted Drug Delivery Application" Spectrochimica Acta Part A: Molecular and Biomolecular Spectroscopy Journal, 148, 146–155. (2015).
30. W. Philipp, J. Jurij, R. Christoph, S. Venkata, T. Claas, W. Ulf, B. Mathias, K. Lorenz, & Stephan B., "Solvent-surface interactions control the phase structure in lasergenerated iron-gold core-shell nanoparticles" Scientific Reports Journal, 6(1), (2016)
31. A.J. Haider, F.I. Sultan, M.J. Haider et al., Spectroscopic and structural properties of zinc oxide nanosphere as random laser medium. Appl. Phys. A **125**, 260 (2019). doi:10.1007/s00339-019-2529-5
32. L. Ma'mani, S. Nikzad, H. Kheiri-Manjili, S. Al-Musawi, M. Saeedi, S. Askarlou, A. Foroumadi, A. Shafiee, Curcumin-loaded guanidine functionalized PEGylated I3ad mesoporous silica nanoparticles KIT-6: Practical strategy for the breast cancer therapy. Eur. J. Med. Chem. **18**, 83:646–654 (2014). doi:10.1016/j.ejmech.2014.06.069
33. S. Al-Musawi, S. Albukhaty, H. Al-Karagoly, F. Almalki, Design, and Synthesis of Multi-Functional Superparamagnetic Core-Gold Shell Coated with Chitosan and Folate Nanoparticles for Targeted Antitumor Therapy. Nanomaterials 2020, 11, 1. doi: 10.3390/nano11010032
34. S. Al-Musawi, A.J. Hadi, S.J. Hadi, N.K.K. Hindi, Preparation and Characterization of Folated Chitosan-Magnetic Nanocarrier for 5-Fluorouracil Drug Delivery and Studying its Effect in Bladder Cancer Therapy. J. Global Pharma Tech. **11**(7), 628–637 (2019)
35. M.A. Al-Kinani, A.J. Haider, S. Al-Musawi, High Uniformity Distribution of Fe@Au Preparation by a Micro-Emulsion Method. IOP Conf. Ser. : Mater. Sci. Eng. **987**, 012013 (2020). doi:10.1088/1757-899X/987/1/012013

Supplemental Data

Supplementary Figure 1 is not available with this version.

Figures

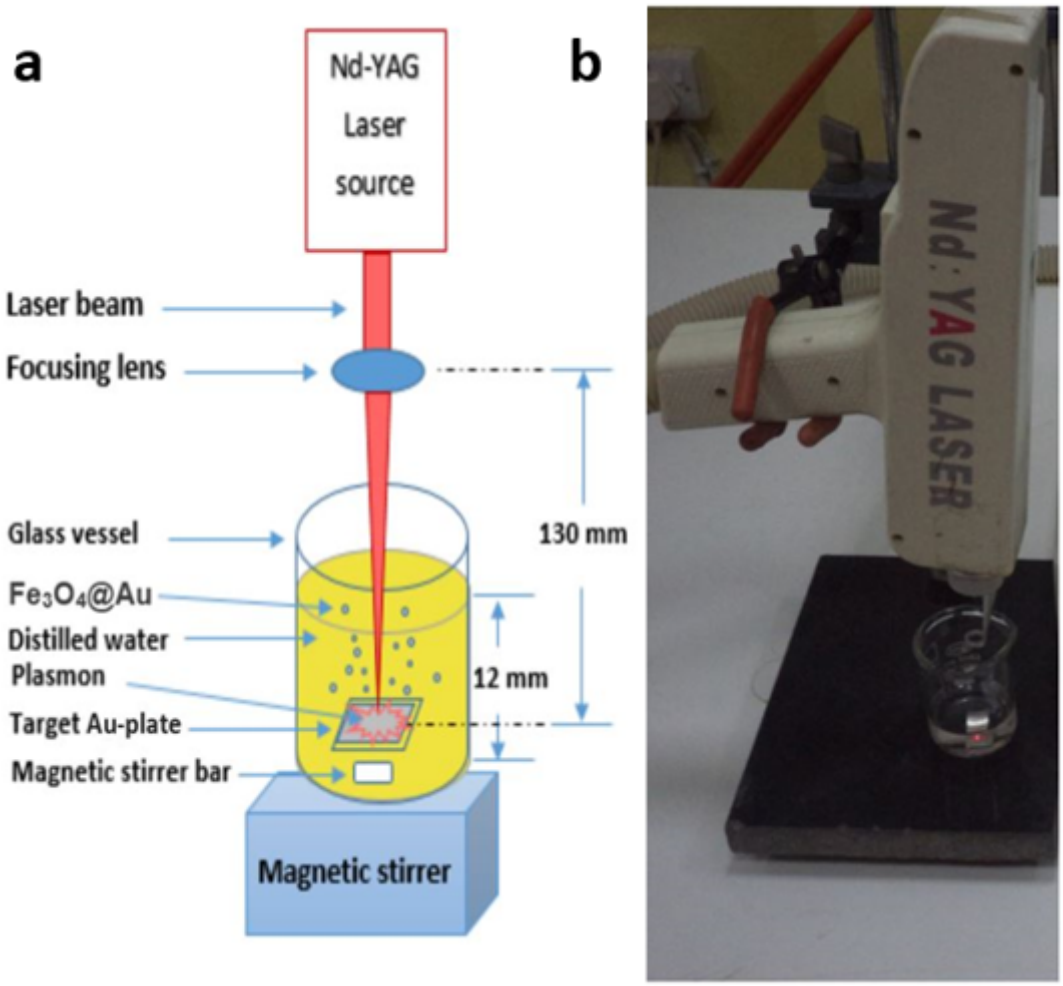

Figure 1

Synthesis process of Fe_3O_4@Au core-shell NPs using PLAL method.

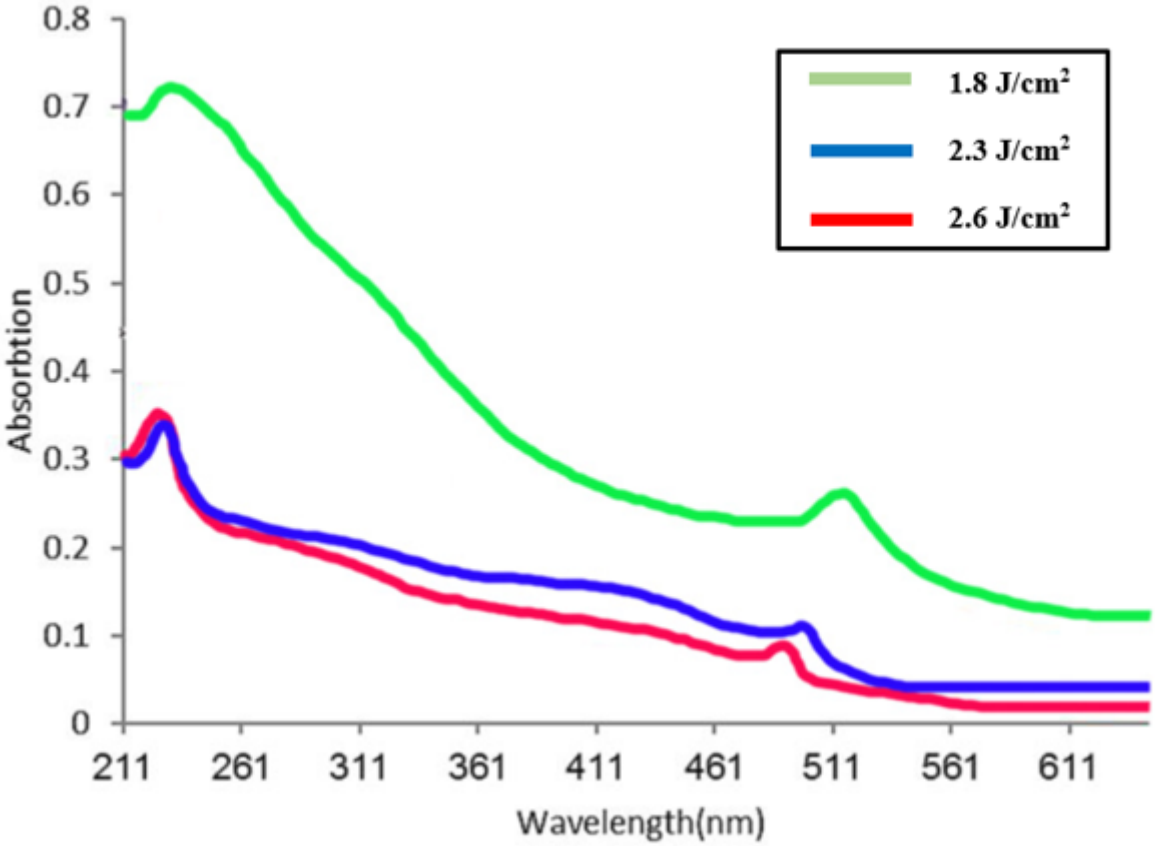

Figure 2

Absorption spectrum of Fe_3O_4@Au NPs with different laser fluence (1.8, 2.3, and 2.6) J/cm^2

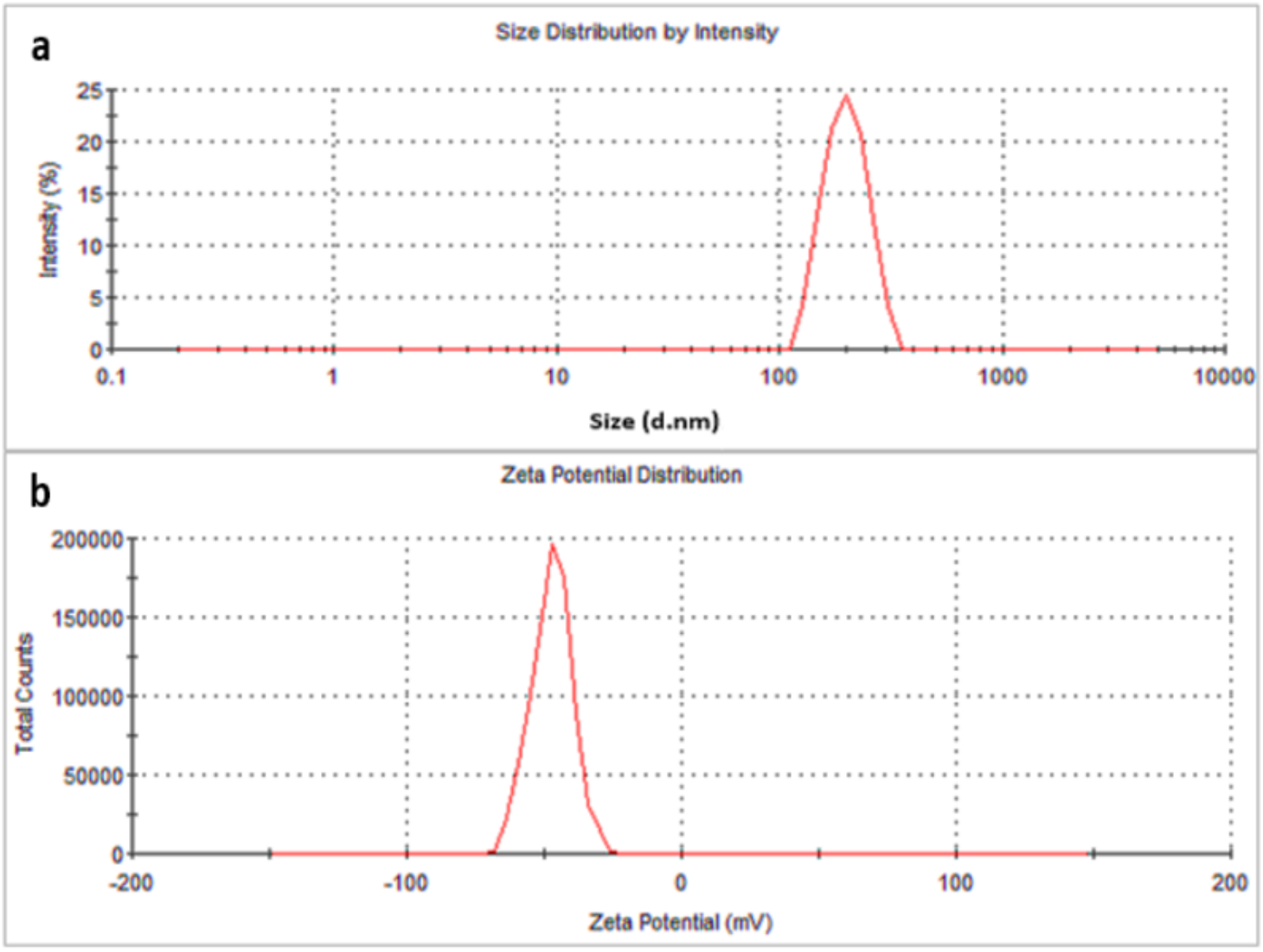

Figure 3

The Fe_3O_4@Au-CS-CU-Fol size (a) and charge (b) using DLS.

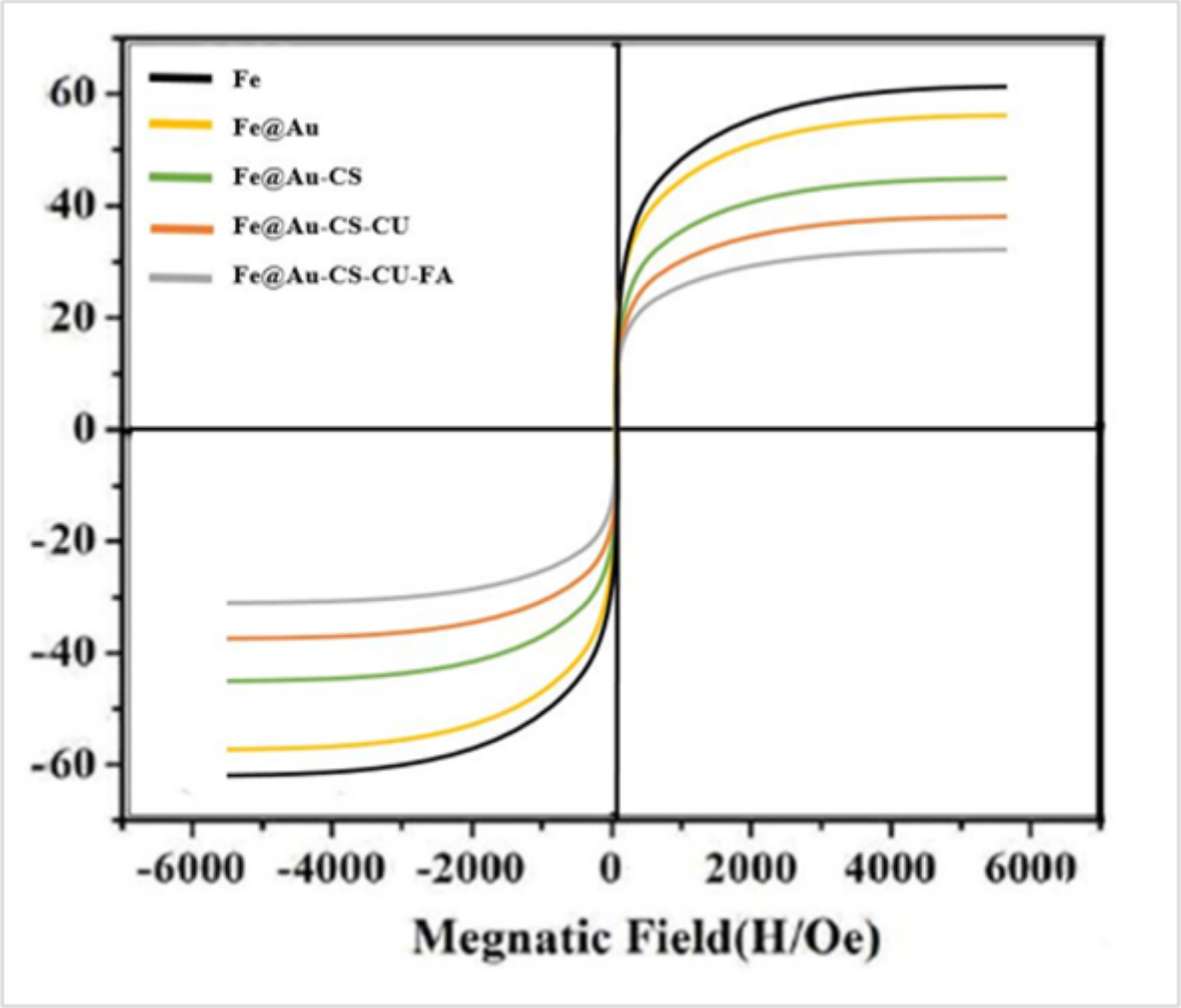

Figure 4

The Magnetisation curve loop of Fe_3O_4, Fe_3O_4@Au, Fe_3O_4@Au-CS, Fe_3O_4@Au-CS-CU, and Fe_3O_4@Au-CS-CU-Fol at 300 K.

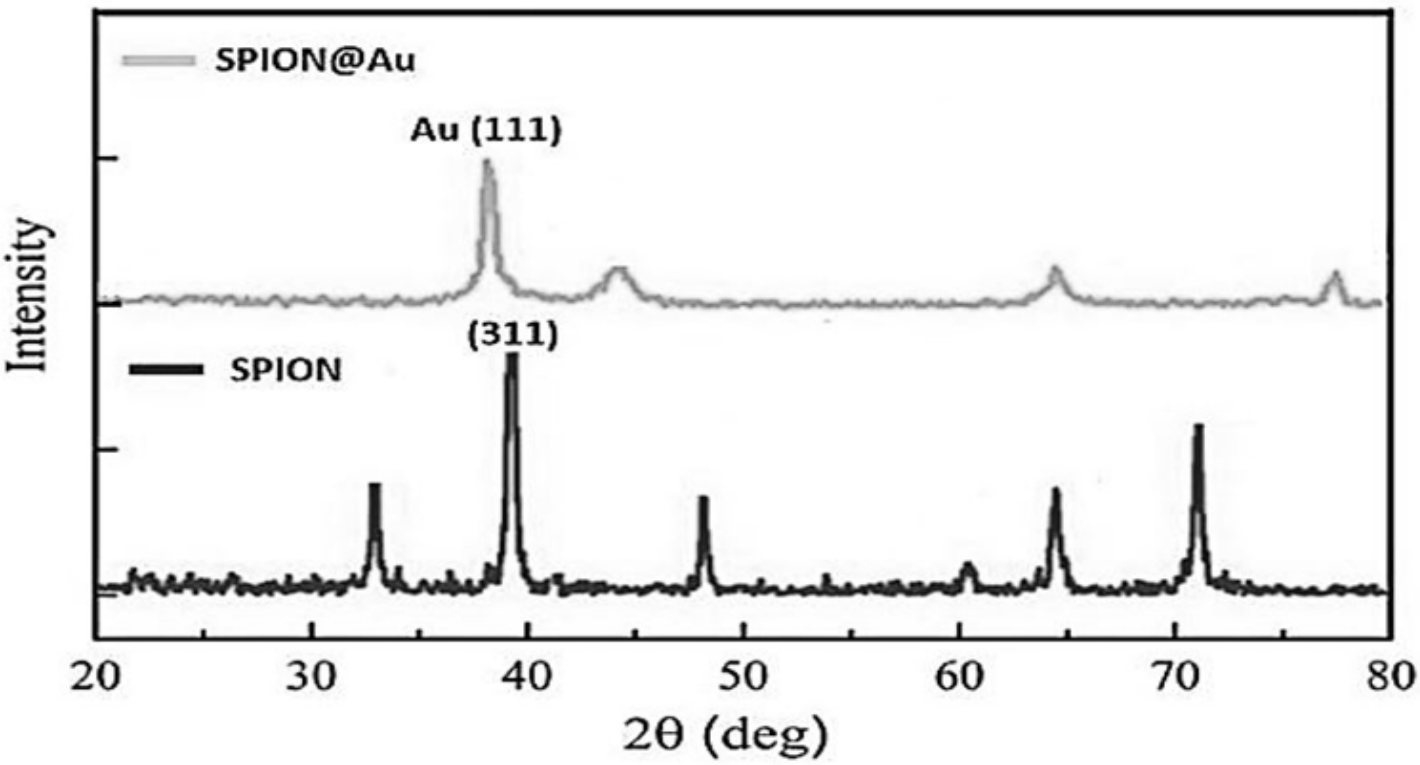

Figure 5

The XRD characterization of the prepared SPION@Au core-shell NPs.

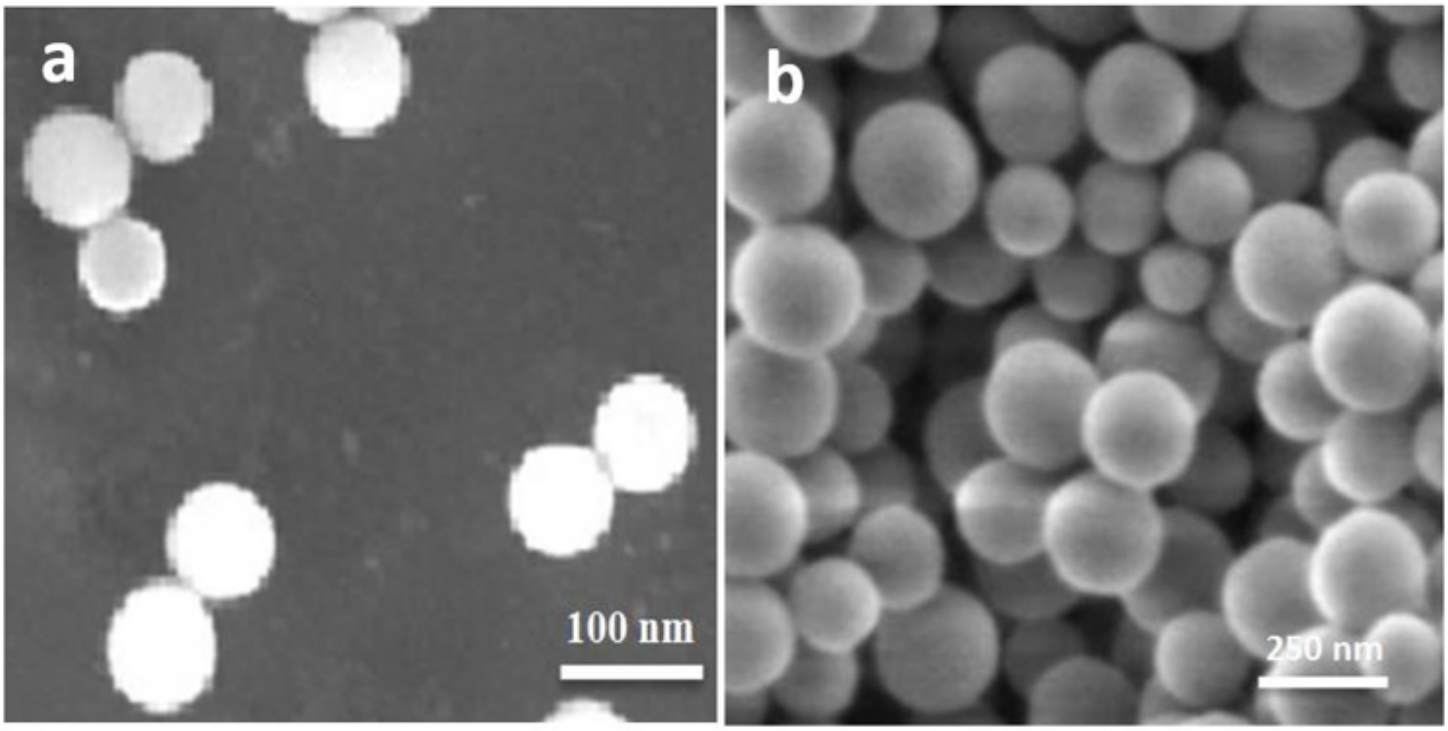

Figure 6

SEM images of (a) Fe_3O_4@Au NPs (b) Fe_3O_4@Au-CS-CU-Fol nanosystem.

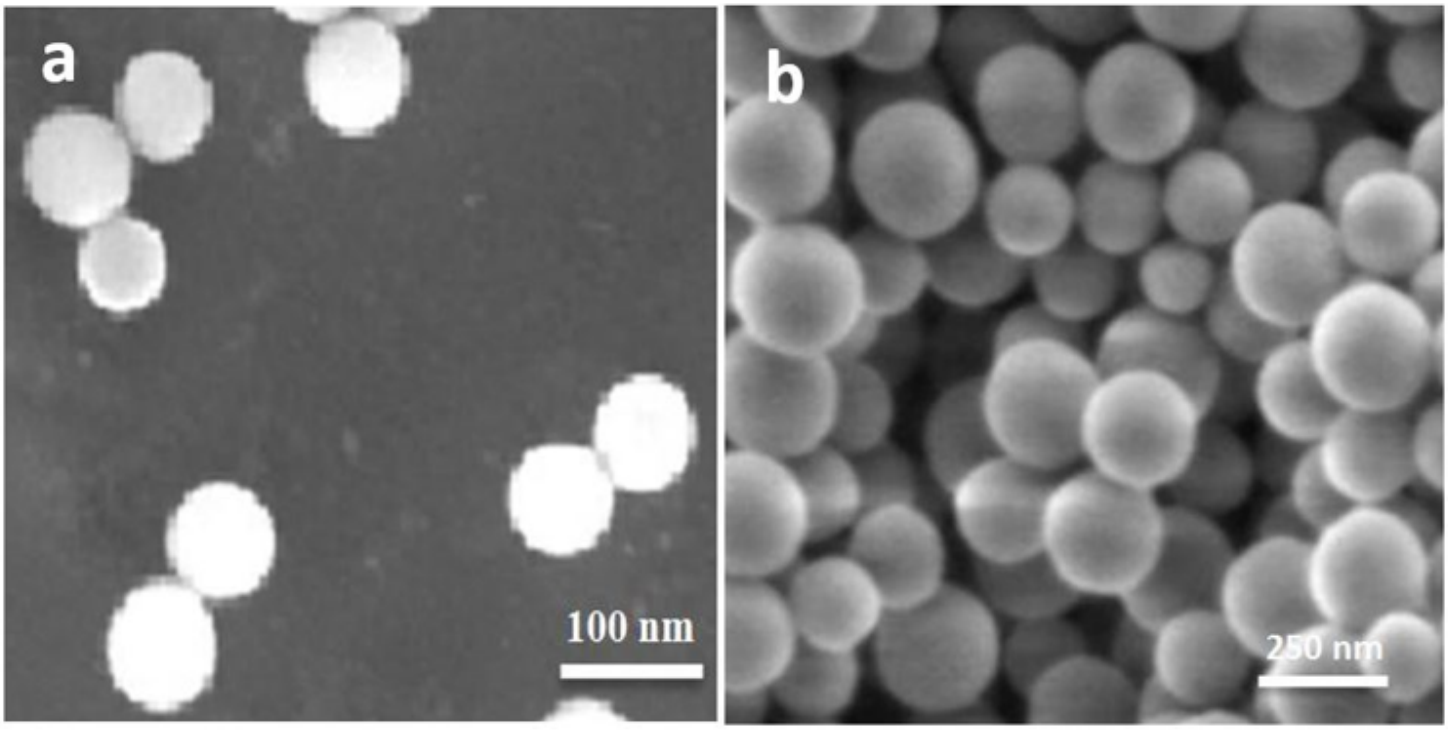

Figure 7

TEM images of (a) Fe_3O_4@Au NPs (b) Fe_3O_4@Au-CS-CU-Fol nanosystem.

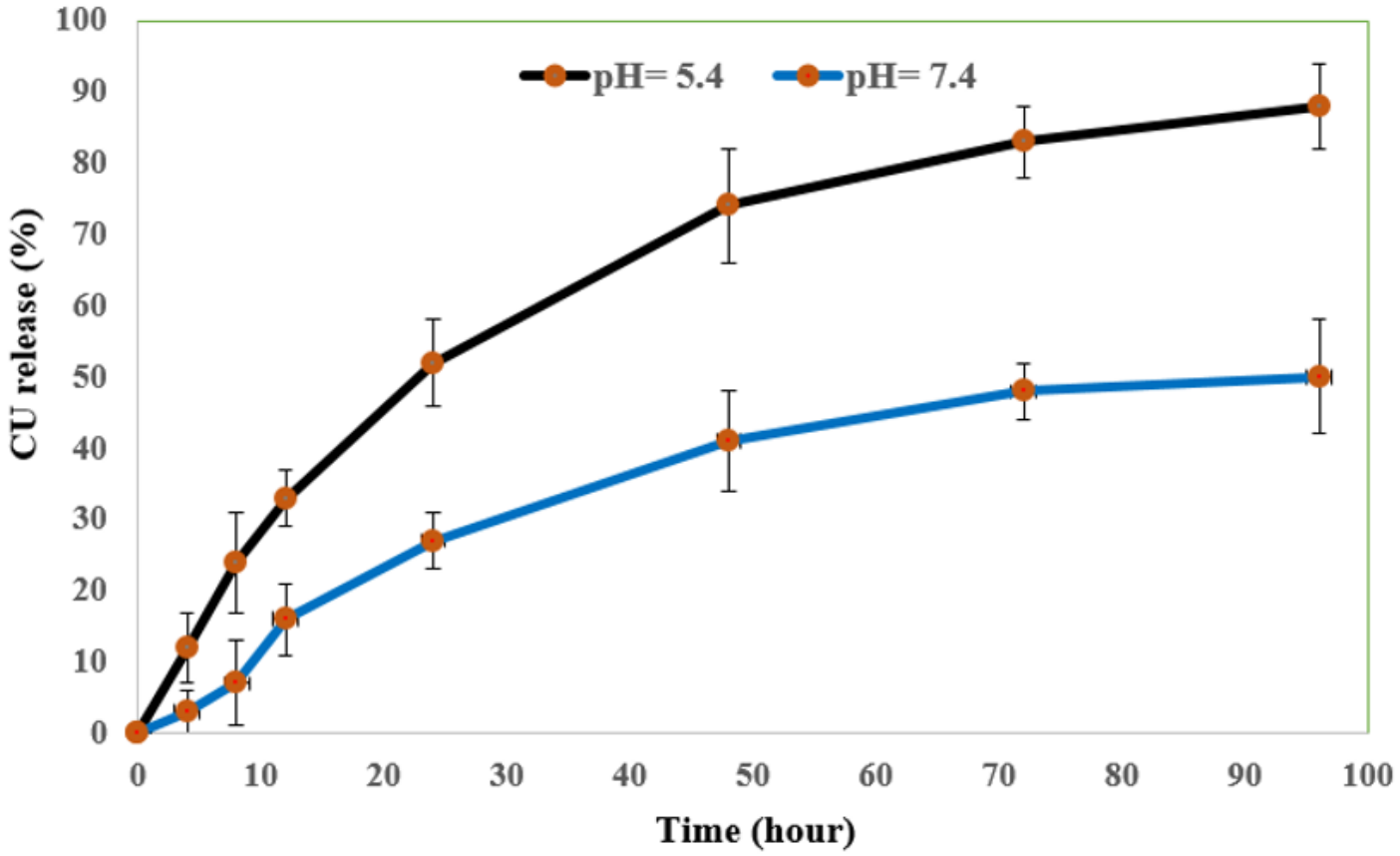

Figure 8

Drug release profile from Fe_3O_4@Au-CS-CU-Fol nanosystem in pH 5.4 and 7.4.

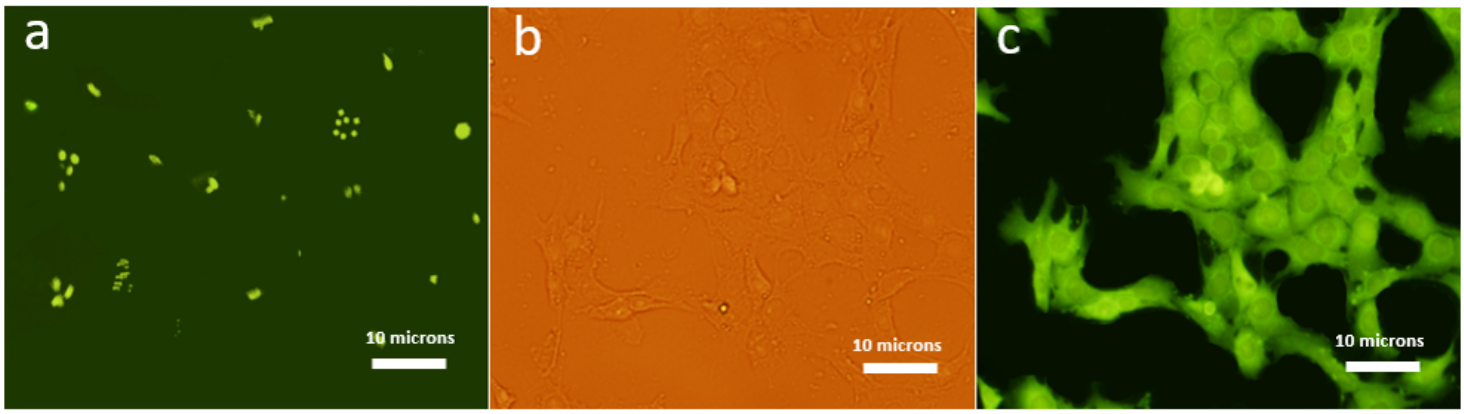

Figure 9

Study of Cell uptake profile of free CU and its nanoformulation (Fe_3O_4@Au-CS-CU-Fol) in MDA-MB-231 cell line via fluorescence microscope (400× magnification). Fluorescence microscopy of cells treated with CU (A) Optic microscopy of cells treated with Fe_3O_4@Au-CS-CU-Fol (B). and Fluorescence microscopy of cells treated with Fe_3O_4@Au-CS-CU-Fol NPs (C).

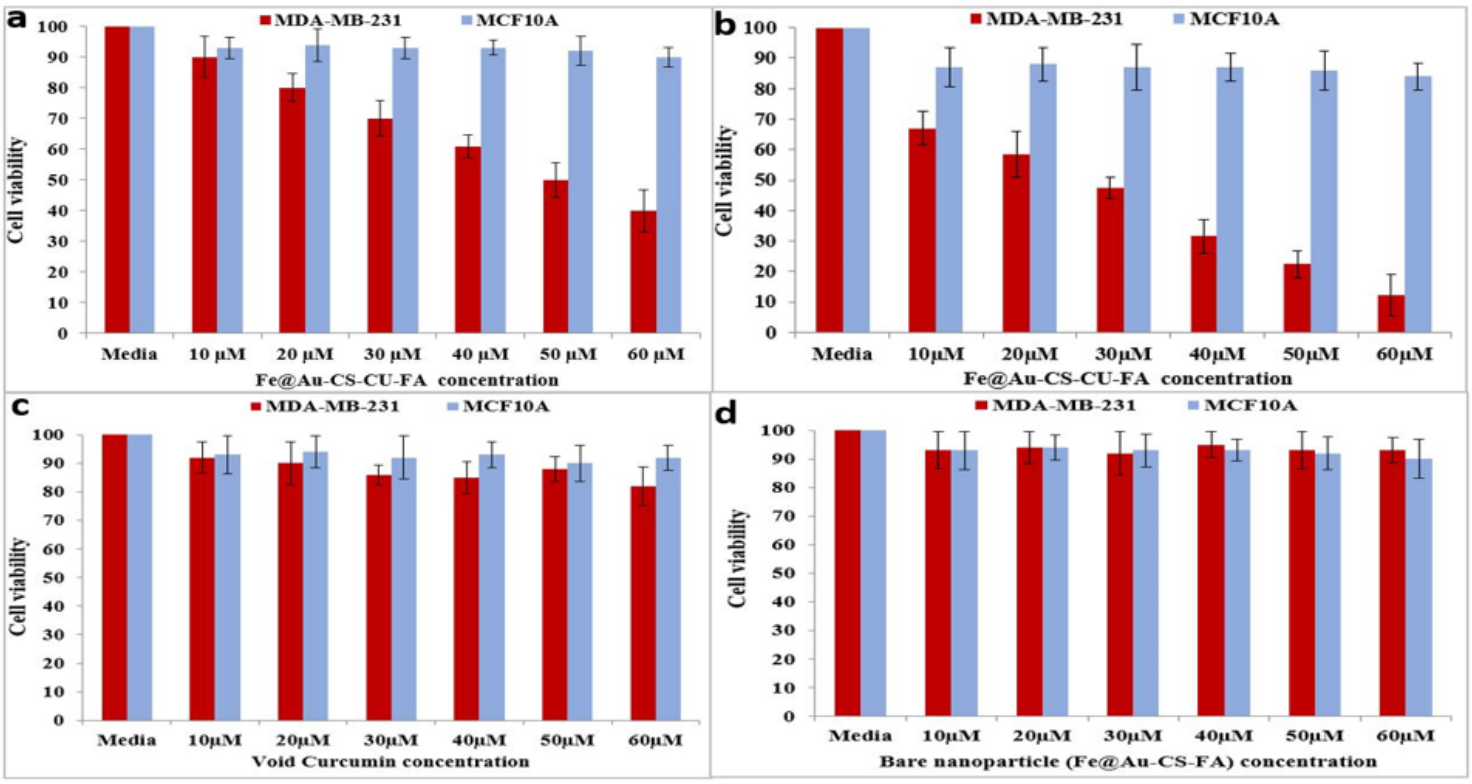

Figure 10

Cell viability rate of different doses of treated drug-loaded nanoformulation after 24 h (A), 48 h (B), and free CU (C) & bare unloaded NPs (D) at 48 h on MDA-MB-231 and MCF10A cell lines.

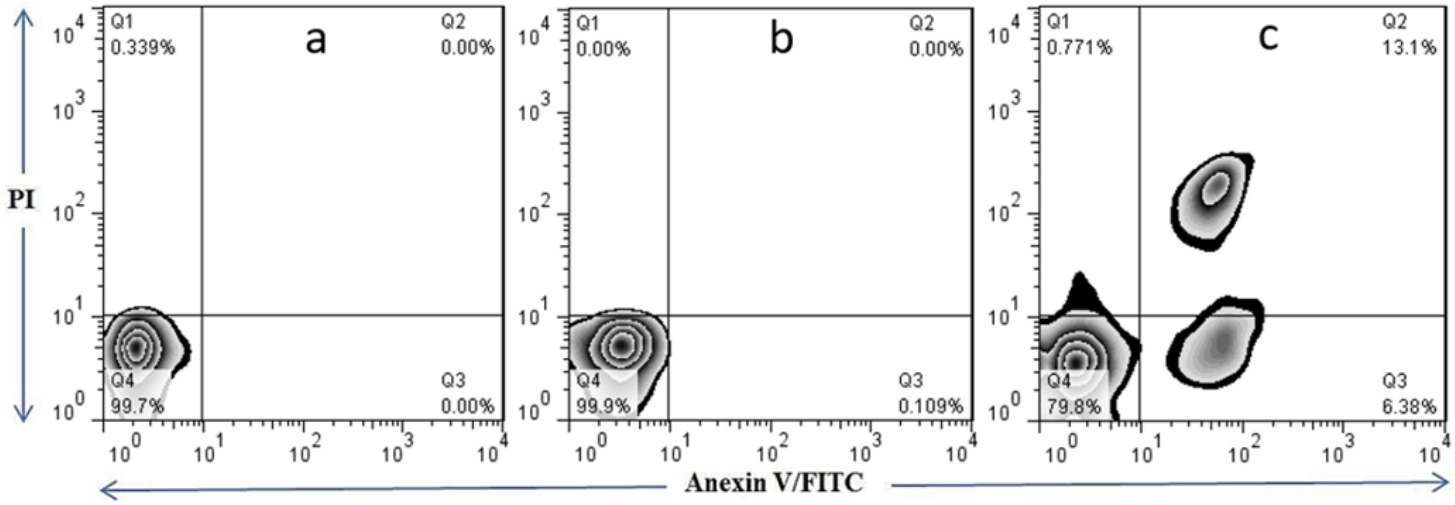

Figure 11

Apoptosis studies by Fe_3O_4@Au-CS-CU-Fol nanosystem (A), Fe_3O_4@Au-CS-Fol nanocarrier (B), free CU (C) on the MDA-MB-231 cell line.

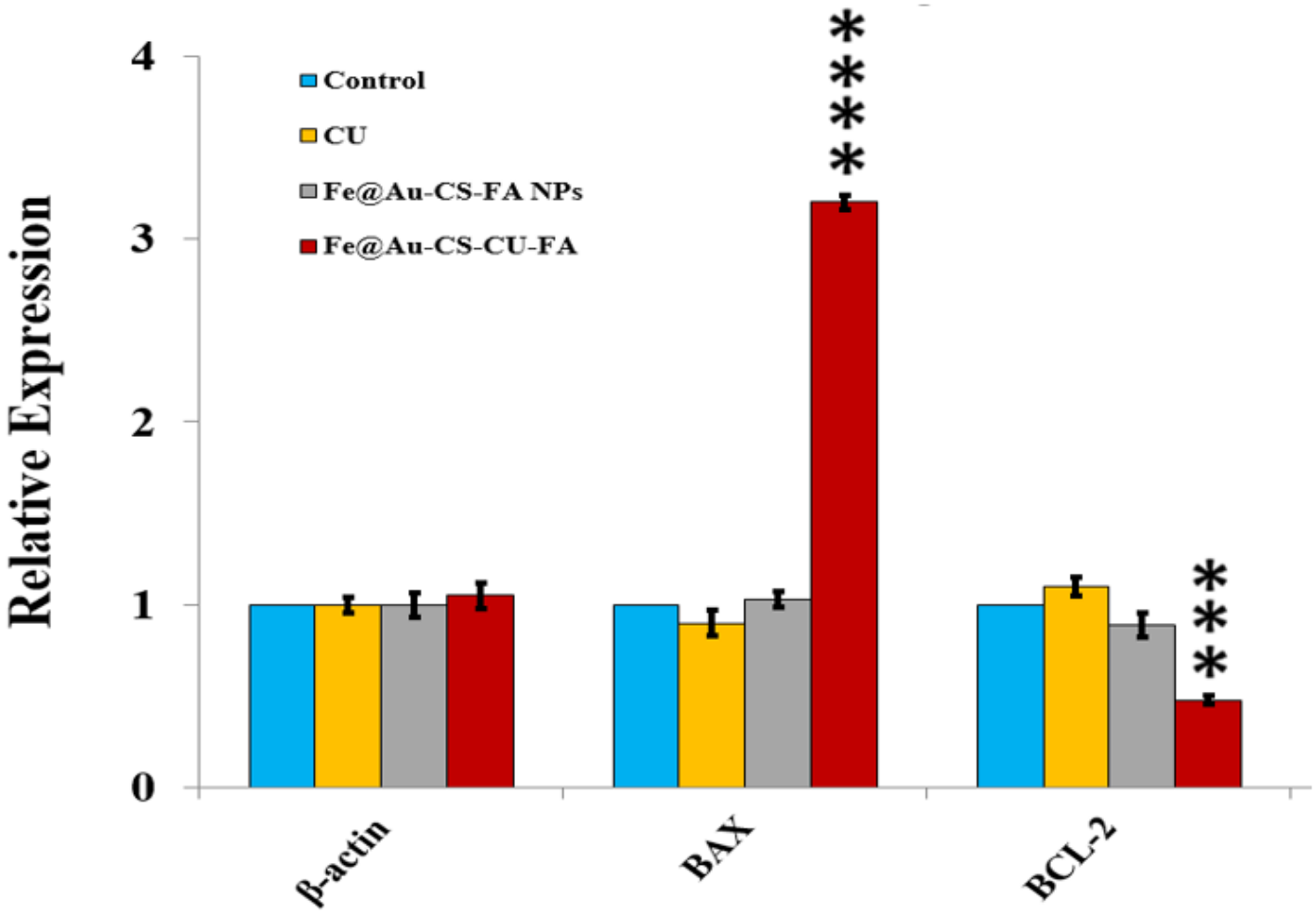

Figure 12

BAX and BCL-2 gene expression study using RT PCR. The MDA-MB-231 cell line was treated with void CU, Fe_3O_4@Au-CS-CU-Fol, and Fe_3O_4@Au-CS-Fol, and BAX and BCL-2 gene expression levels were evaluated by real-time PCR. The results were two-way ANOVA and Bonferroni post-test. (mean±SD (n=3), ***P<0.001, ****P<0.0001).

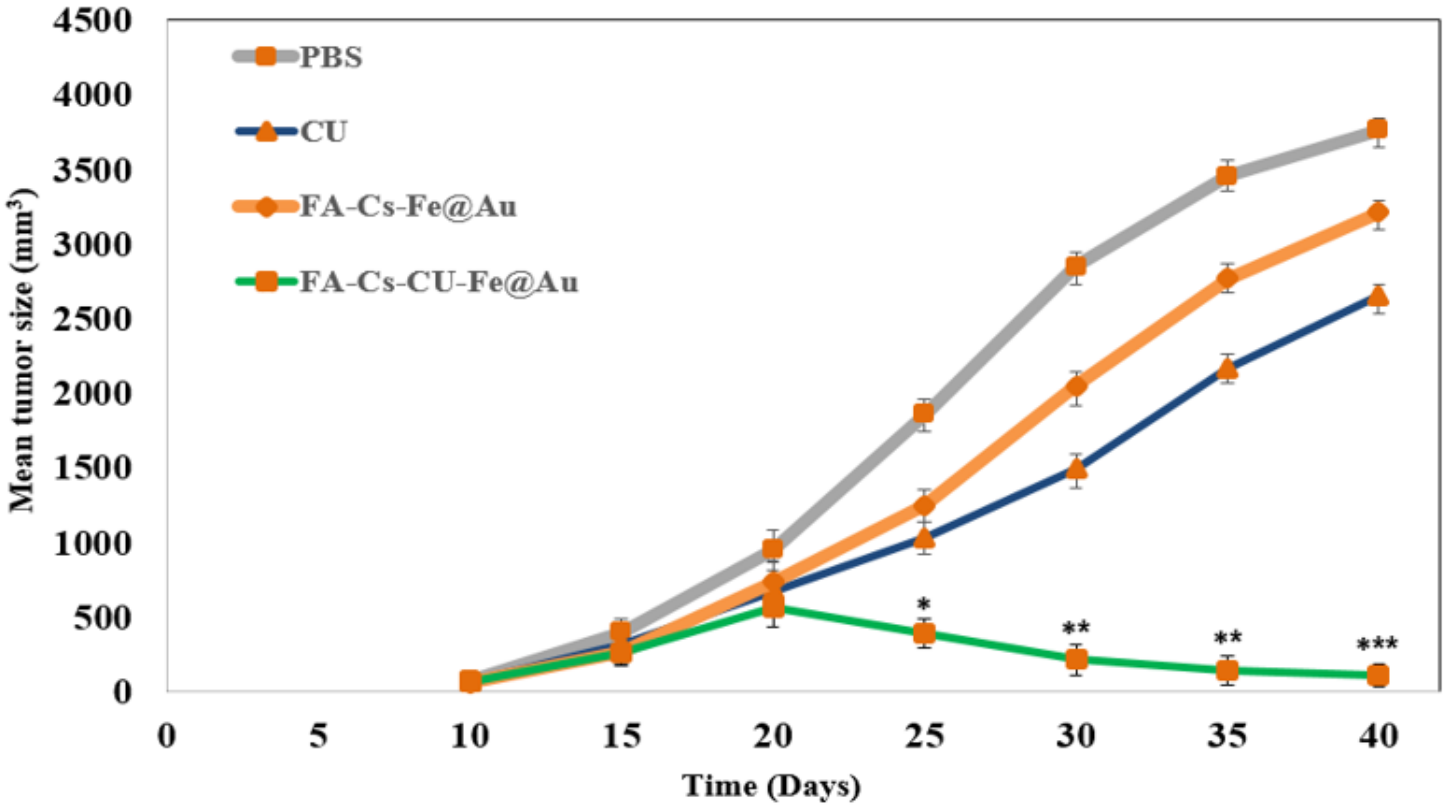

Figure 13

The tumor volume curve of mice bearing tumor (MDA-MB-231).